Journal of
Marine Science and Engineering

MDPI

Article

Model Predictive Control of Counter-Rotating Motors for Underwater Vehicles Considering Unbalanced Load Variation

Shukuan Zhang [1,*], Yunxiang Nan [1], Yusen Zhang [1], Chuan Xiang [1] and Mai The Vu [2,*]

[1] College of Marine Electrical Engineering, Dalian Maritime University, Dalian 116026, China
[2] Department of Intelligent Mechatronics Engineering, Sejong University, Seoul 05006, Republic of Korea
* Correspondence: zhangshukuan@dlmu.edu.cn (S.Z.); maithevu90@sejong.ac.kr (M.T.V.)

Abstract: The propulsion system for underwater vehicles, driven by a counter-rotating permanent magnet synchronous motor (CRPMSM), can enhance the operational stability and efficiency of the vehicle. Due to the influence of complex underwater flows, the load imbalance of CRPMSM's dual counter-rotating rotors may lead to severe issues of dual-rotor desynchronization rotation. Combining traditional vector control (VC) with master-slave control strategies can address the desynchronization problem when CRPMSM's load changes. However, it results in significant speed fluctuations and a long transition time during the transition from load disturbance to synchronous rotation. This paper introduces a model predictive control (MPC) strategy to effectively resolve this issue. The incremental MPC model is established based on the mathematical model of CRPMSM in the *dq* coordinate system. The predictive control system forecasts the *d*- and *q*-axis components of stator currents for the next four control cycles. It selects the optimal control increments to minimize the cost function based on current predictions and different inverter voltage states. The obtained optimal *d*- and *q*-axis components of stator voltage are used to control CRPMSM under unbalanced load disturbances. Simulation results demonstrate that, compared to the VC strategy, CRPMSM utilizing the MPC strategy exhibits better dynamic performance with faster speed response and reduced torque fluctuations during load and speed variations.

Keywords: counter-rotating permanent magnet synchronous motor; model predictive control; underwater vehicle; unbalanced load

check for updates

Citation: Zhang, S.; Nan, Y.; Zhang, Y.; Xiang, C.; Vu, M.T. Model Predictive Control of Counter-Rotating Motors for Underwater Vehicles Considering Unbalanced Load Variation. *J. Mar. Sci. Eng.* **2024**, *12*, 330. https://doi.org/10.3390/jmse12020330

Academic Editor: Eugen Rusu

Received: 15 January 2024
Revised: 8 February 2024
Accepted: 13 February 2024
Published: 15 February 2024

Correction Statement: This article has been republished with a minor change. The change does not affect the scientific content of the article and further details are available within the backmatter of the website version of this article.

Copyright: © 2024 by the authors. Licensee MDPI, Basel, Switzerland. This article is an open access article distributed under the terms and conditions of the Creative Commons Attribution (CC BY) license (https://creativecommons.org/licenses/by/4.0/).

1. Introduction

Ocean exploitation has become a strategic target for nations due to its abundant mineral resources, biological resources, and energy resources. Advanced marine equipment plays a crucial role in the exploration and utilization of these resources. Underwater vehicles are particularly essential in deep-sea resource surveying and development. The streamlined structures of underwater vehicles generate significant unidirectional rolling moments, causing yawing during high-speed navigation. Using a single-propeller propulsion system exacerbates this yawing, potentially leading to capsizing [1,2]. Employing a counter-rotating propeller propulsion system composed of two coaxial counter-rotating propellers generates opposite and canceling rotational torques, ensuring the stability of the vehicle. Furthermore, the energy generated by the front propeller's wake can be recovered and utilized by the rear propeller, improving the efficiency of the propulsion system [3].

A counter-rotating permanent magnet synchronous motor (CRPMSM) can be regarded as two PMSMs connected in series, offering advantages such as high power density and efficiency, making it particularly suitable for driving the counter-rotating propellers. However, the control strategy for CRPMSM with dual rotors is complex. CRPMSM is susceptible to underwater flow disturbances, and the load torques of the two rotors may become imbalanced, resulting in issues like motor desynchronization and vehicle power loss. Therefore, the investigation of control strategies for CRPMSM under unbalanced load conditions is of significant practical importance.

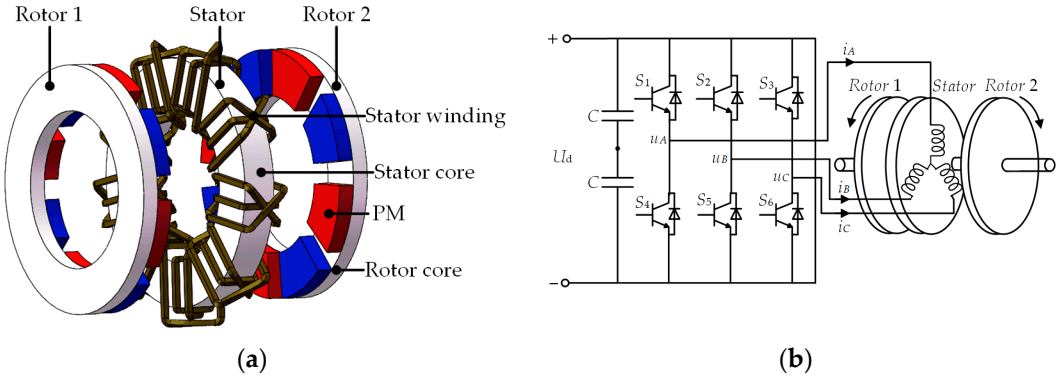
The control strategy for CRPMSM is similar to that of controlling multiple motors using a single inverter [4–9]. Both traditional vector control (VC) and direct torque control strategies involve closed-loop control of one rotor while the other rotor follows freely, which can lead to desynchronization when the load of the two rotors becomes imbalanced. Based on traditional VC, Cheng et al. proposed a closed-loop control strategy for dual rotors that can achieve synchronous rotation [10]. However, it faces the problem of significant speed fluctuations during the transition from load disturbance to equilibrium. Rao et al. introduced torque-sharing control for dual rotors, allowing them to operate synchronously under minor unbalanced loads [11]. Nevertheless, the operation of the motor under severe, unbalanced load conditions is not investigated. Zhong et al. presented a dynamic master-slave control strategy based on traditional VC, enabling CRPMSM to synchronize under unbalanced loads [12]. However, it still exhibited significant speed fluctuations during speed adjustment.

Traditional control strategies cannot guarantee the dynamic performance of the CRPMSM. Researchers have proposed non-linear control methods such as sliding mode control [13,14], robust control [15,16], and intelligent control [17,18] to improve the control performance of CRPMSM. Luo et al. introduced an improved VC strategy with load torque compensation to address the issue of significant speed fluctuations during CRPMSM speed adjustment [19]. Luo et al. employed fuzzy torque control based on the torque-angle phase difference of CRPMSM to improve speed and torque stability when the load is unbalanced [20]. The study of speed control for PMSM under sudden disturbance loads provides theoretical references for CRPMSM control under unbalanced load conditions [21]. Zhang et al. proposed disturbance observers and composite terminal sliding mode control into PMSM speed control systems, reducing motor speed variations during sudden disturbance loads [22].

By adopting the dynamic master-slave control strategy, CRPMSM can achieve synchronous rotation of the two rotors under unbalanced loads, but it still exhibits significant speed fluctuations during speed regulation. To address this issue, this paper proposes a model predictive control (MPC) strategy based on dynamic master-slave control to reduce speed fluctuations in CRPMSM under unbalanced loads. Firstly, the mathematical model of CRPMSM is deduced from the dq coordinate system. Secondly, the dynamic master-slave control strategy is employed to orient the rotor flux according to the quantitative relationship between the load torque of dual rotors. Then, through model prediction, feedback correction, and rolling optimization of the model, combined with dynamic master-slave control, the paper achieves speed control of CRPMSM under unbalanced loads. Finally, simulation models of CRPMSM with MPC and VC are established, respectively, to simulate the speed, torque, and phase current of CRPMSM under various operating conditions. Compared to traditional VC, the proposed method allows the two rotors to synchronize their speed in a shorter time under load imbalance, resulting in smaller speed and torque fluctuations for CRPMSM.

2. Mathematical Model of CRPMSM

The CRPMSM under study is an axial magnetic flux structure composed of two rotors positioned on either side and a stator in the middle, as illustrated in Figure 1. The stator core has an equal number of stator slots on both sides. By cross winding B-phase coil and C-phase coil at both sides of stator slots, two sets of three-phase stator windings with ABC-phase sequence at one side of the stator and ACB-phase sequence at another side are obtained, respectively. Both rotors have a surface-mounted permanent magnet structure with the same number of rotor pole pairs. When three-phase balanced AC currents are applied to the stator winding, two rotating magnetic fields with opposite directions and equal speeds are generated. The interaction between the armature magnetic field and the adjacent PM magnetic field produces electromagnetic torques in opposite directions, thereby driving the two rotors to counter-rotate.



(**a**) (**b**)

Figure 1. CRPMSM diagram. (**a**) CRPMSM structure. (**b**) CRPMSM with control diagram.

CRPMSM can be regarded as two PMSMs with identical parameters connected in series, and the mathematical model can be derived from the mathematical model of PMSM. Assuming that only one rotor of CRPMSM is rotating and considering the coupling relationship between this rotor and the stator, the mathematical model of CRPMSM can be expressed using the mathematical model of PMSM. Rotor 1 and Rotor 2 represent the two rotors of CRPMSM, and separate mathematical models for CRPMSM in the dq coordinate system are established when considering the rotation of a single rotor.

The following assumptions are made in the establishment of the CRPMSM mathematical model: (1) The saturation effect of both stator and rotor cores is ignored. (2) The influence of temperature rise on stator resistance is neglected. (3) The magnetic fields generated by the permanent magnet and armature winding in the air-gap are sinusoidal. (4) The no-load back EMF induced by the armature winding is considered sinusoidal.

The stator voltage equations can be expressed as

$$u_{d1} = R_s i_{d1} + L_{d1}\frac{di_{d1}}{dt} - \omega_1 L_{q1} i_{q1} \tag{1}$$

$$u_{q1} = R_s i_{q1} + L_{q1}\frac{di_{q1}}{dt} + \omega_1 L_{d1} i_{d1} + \omega_1 \psi_{f1} \tag{2}$$

$$u_{d2} = R_s i_{d2} + L_{d2}\frac{di_{d2}}{dt} - \omega_2 L_{q2} i_{q2} \tag{3}$$

$$u_{q2} = R_s i_{q2} + L_{q2}\frac{di_{q2}}{dt} + \omega_2 L_{d2} i_{d2} + \omega_2 \psi_{f2} \tag{4}$$

where u_{d1}, u_{q1}, i_{d1}, and i_{q1} are the components of stator voltage and current on the d- and q-axes of Rotor 1; u_{d2}, u_{q2}, i_{d2}, and i_{q2} are the components of stator voltage and current on the d- and q-axes of Rotor 2; Ψ_{f1} and Ψ_{f2} are the magnetic flux linkages of Rotor 1 and Rotor 2, and due to the symmetry of CRPMSM's two rotors, $\Psi_{f1} = \Psi_{f2} = \Psi_f$; ω_1 and ω_2 are the electrical angular velocities of Rotor 1 and Rotor 2; and L_{q1}, L_{d1}, L_{q2}, and L_{d2} are the d- and q-axis inductances on the rotor 1 and rotor 2 sides, with $L_{d1} = L_{d2}$ and $L_{q1} = L_{q2}$.

The electromagnetic torque of the rotor can be expressed as

$$T_{e1} = \frac{3}{2} p \psi_{f1} i_{q1} \tag{5}$$

$$T_{e2} = \frac{3}{2} p \psi_{f2} i_{q2} \tag{6}$$

where T_{e1}, T_{e2} are the electromagnetic torques of Rotor 1 and Rotor 2; p is the number of pole pairs.

The motion equation of two rotors can be expressed as

$$J_1\frac{d\omega_1}{dt} = T_{e1} - T_{L1} \tag{7}$$

$$\omega_1 = \frac{d\theta_1}{dt} \tag{8}$$

$$J_2 \frac{d\omega_2}{dt} = T_{e2} - T_{L2} \tag{9}$$

$$\omega_2 = \frac{d\theta_2}{dt} \tag{10}$$

where T_{L1}, T_{L2} are load torques of Rotor 1 and Rotor 2; θ_1, θ_2 are position angles of Rotor 1 and Rotor 2; J_1, J_2 are moments of inertia of Rotor 1 and Rotor 2.

Furthermore, CRPMSM can be considered a series connection of two PMSMs with identical parameters, and the current relationship between the two motors is expressed as

$$i_{d1} = i_{d2} = i_d \tag{11}$$

$$i_{q1} = i_{q2} = i_q \tag{12}$$

The voltage relationship between the two motors is expressed as

$$u_d = u_{d1} + u_{d2} \tag{13}$$

$$u_q = u_{q1} + u_{q2} \tag{14}$$

Therefore, the mathematical model of CRPMSM with the consideration of dual rotor rotation can be obtained. The stator voltage equations can be written as

$$u_d = 2R_s i_d + 2L_d \frac{di_d}{dt} - L_q i_q(\omega_1 + \omega_2) \tag{15}$$

$$u_q = 2R_s i_q + 2L_q \frac{di_q}{dt} + L_d i_d(\omega_1 + \omega_2) + \psi_f(\omega_1 + \omega_2) \tag{16}$$

The electromagnetic torque can be written as

$$T_{e1} = T_{e2} = \frac{3}{2} p \psi_f i_q \tag{17}$$

3. Master-Slave Control Strategy for CRPMSM

In an ideal scenario, the electromagnetic torque of both rotors of CRPMSM is equal to the load torque. In this situation, when controlling CRPMSM using a single inverter with the $i_d = 0$ control method, the d-axis of the rotating coordinate system should be aligned with the direction of the rotor magnetic flux. Orienting the d-axis to either Ψ_{f1} or Ψ_{f2} and only one rotor needs to be closed-loop controlled to achieve dual rotor synchronous rotation. Under these conditions, based on the motion equations of CRPMSM, it can be concluded that $\omega_1 = \omega_2 = \omega$, and $\theta_1 = \theta_2 = \theta$. Figure 2 illustrates the phasor diagram of CRPMSM when the load torques of both rotors are balanced. The magnetic fluxes Ψ_{f1} and Ψ_{f2} of both rotors align with the d-axis direction, and the torque angles of both rotors satisfy $\delta_1 = \delta_2 = 90^\circ$.

However, in practical situations, uncontrollable disturbances like ocean waves and vortexing can lead to unequal load torques on both rotors, resulting in $\omega_1 \neq \omega_2$ and $\theta_1 \neq \theta_2$. If the load torque T_{L1} on Rotor 1 is greater than T_{L2} on Rotor 2, then the position angle θ_1 of Rotor 1 is less than the position angle θ_2 of Rotor 2. Conversely, if $T_{L1} < T_{L2}$, then $\theta_1 > \theta_2$. In such cases, if the d-axis is continuously oriented to either Ψ_{f1} or Ψ_{f2} during the control process, it may lead to a desynchronization problem between the two rotors. Taking the orientation to the direction of Ψ_{f1} as an example, the stability of CRPMSM will be discussed under two scenarios in cases of load imbalance: $T_{L1} > T_{L2}$ and $T_{L1} < T_{L2}$.

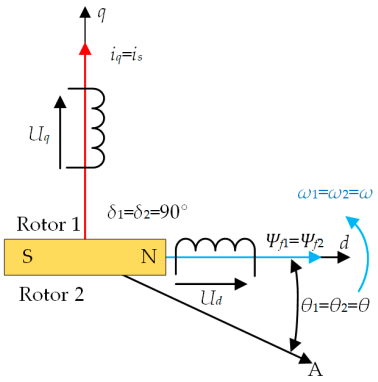


Figure 2. Phasor diagram of CRPMSM under balanced load.

(1) The case of $T_{L1} > T_{L2}$

In this case, the phasor diagram of both rotors of CRPMSM is shown in Figure 3, where Ψ_{f2} leads Ψ_{f1}, and the torque angle δ_2 of the motor is between 0° and 90°. According to Equation (17), the electromagnetic torque of both rotors can be expressed as follows:

$$T_{e1} = \frac{3}{2} p \psi_f i_q \tag{18}$$

$$T_{e2} = \frac{3}{2} p \psi_f i_q sin\delta_2 \tag{19}$$

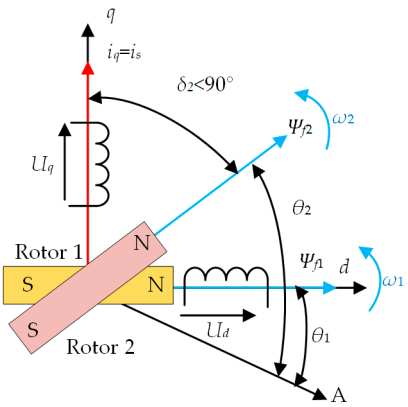


Figure 3. Phasor diagram of CRPMSM in the case of $T_{L1} > T_{L2}$.

Since the *d*-axis of the rotating *dq* coordinate is oriented to Ψ_{f1}, Rotor 1 is under closed-loop control, and the armature current of Rotor 2 is forced to be the same as that of Rotor 1. When Rotor 1 stably rotates, $T_{e1} = T_{L1}$. According to the motion equation of Rotor 2, the position angle θ_2 of Rotor 2 increases as the load torque on Rotor 2 decreases, leading to a decrease in the torque angle δ_2. The electromagnetic torque T_{e2} of Rotor 2 decreases as δ_2 decreases, and at this point, $T_{e2} < T_{e1}$ and $T_{e1} = T_{L1}$. Finally, as δ_2 decreases further, T_{e2} gradually decreases until it reaches equilibrium with T_{L2} again, achieving synchronous rotation of both rotors of the CRPMSM when the load is unbalanced.

(2) The case of $T_{L1} < T_{L2}$

In this case, Ψ_{f2} lags behind Ψ_{f1}, and the torque angle δ_2 of Rotor 2 is greater than 90°, as the phasor diagram of both rotors of CRPMSM is shown in Figure 4. The electromagnetic torque equations for both rotors can still be expressed as Equations (18) and (19). When Rotor 1 stably rotates, it satisfies that $T_{e1} = T_{L1}$. According to the motion equation of Rotor 2, as the load torque on Rotor 2 increases, the position angle θ_2 of Rotor 2 and the torque angle δ_2 both increase, causing a decrease in the electromagnetic torque T_{e2}. At this point,

$T_{e2} < T_{L2}$, and T_{e2} cannot reach equilibrium with T_{L2}, making it impossible for both rotors of CRPMSM to synchronize when the load is unbalanced.

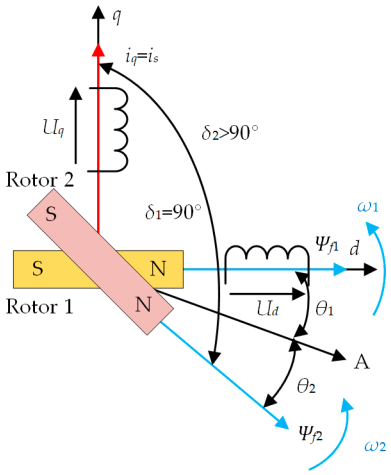


Figure 4. Phasor diagram of CRPMSM in the case of $T_{L1} < T_{L2}$.

It can be found that if a certain rotor flux is always selected as the d-axis orientation for both rotors during the CRPMSM control process, the problem of dual rotors out of step may occur when the load is unbalanced. To address this issue, when $T_{L1} < T_{L2}$, it is advisable to orient the d-axis to Ψ_{f2} instead of Ψ_{f1}, as shown in Figure 5. In this case, δ_2 equals 90°, and δ_1 is less than 90°. The torque equations for two rotors can be expressed as follows:

$$T_{e1} = \frac{3}{2} p \psi_f i_q \sin \delta_1 \tag{20}$$

$$T_{e2} = \frac{3}{2} p \psi_f i_q \tag{21}$$

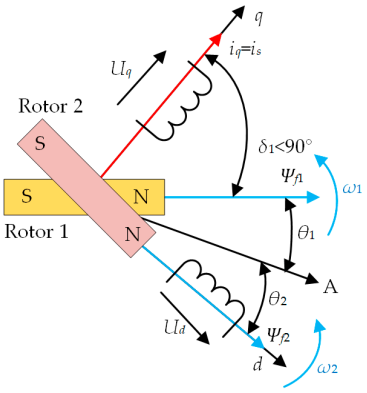


Figure 5. Reoriented phasor diagram of CRPMSM in the case of $T_{L1} < T_{L2}$.

When Rotor 2 stably rotates, it satisfies that $T_{e2} = T_{L2}$. Based on the motion equation and electromagnetic torque equation of Rotor 1, the position angle θ_1 of Rotor 1 increases as T_{L1} decreases, and the torque angle δ_1 decreases. Electromagnetic torque T_{e1} also decreases until it reaches equilibrium with T_{L1} again, allowing CRPMSM to achieve synchronous rotation of both rotors when the load is unbalanced.

Therefore, during the control process of CRPMSM, the rotor flux should be dynamically oriented according to the magnitudes of the load torques of both rotors. Specifically, the d-axis in vector control is dynamically aligned to the rotor flux with the larger load torque, which is regarded as the master rotor, while another one is regarded as the slave rotor. The rotor with the larger load torque will have a smaller rotor position angle. Therefore,

the load variations of both rotors can be monitored in real-time by resolvers to determine the master rotor and the slave rotor, thereby achieving coordination control of CRPMSM.

4. Model Predictive Control for CRPMSM

MPC utilizes the current state information of the system as the state variables of the predictive model and the seven inverter switching vectors as the control input variables of the predictive model. The outputs are calculated using the predictive model, while the predictive model is corrected based on the difference between the system output values and the predicted values. Therefore, the predictive results are used to select the optimal voltage vector that best approximates the actual output compared to the predicted output. The model predictive control strategy for CRPMSM is elaborated on in the following section.

4.1. Model Predictive Control Strategy for CRPMSM

The *dq*-axis currents are used as the state variables for the CRPMSM predictive control system. According to the mathematical model of CRPMSM, it can be derived as

$$\begin{cases} \frac{di_d}{dt} = \frac{(\omega_1 L_{q1}+\omega_2 L_{q2})}{L_{d1}+L_{d2}} i_q - \frac{2R_s}{L_{d1}+L_{d2}} i_d + \frac{1}{L_{d1}+L_{d2}} u_d \\ \frac{di_q}{dt} = -\frac{(\omega_1 L_{d1}+\omega_2 L_{d2})}{L_{q1}+L_{q2}} i_d - \frac{2R_s}{L_{q1}+L_{q2}} i_q + \frac{1}{L_{q1}+L_{q2}} u_q - \frac{\omega_1 \psi_{f1}+\omega_2 \psi_{f2}}{L_{q1}+L_{q2}} \end{cases} \tag{22}$$

The output equation of the system is as follows:

$$y = \begin{pmatrix} y_d \\ y_q \end{pmatrix} = \begin{pmatrix} 1 & 0 \\ 0 & 1 \end{pmatrix} \begin{pmatrix} i_d \\ i_q \end{pmatrix} \tag{23}$$

where y_d, y_q are the output variables on the *d*- and *q*-axis.

The MPC system is an optimization system that calculates in a sequential manner within control cycles, and operates as a discrete-time system. Therefore, a first-order Euler discretization is applied to Equation (22) and can be obtained as

$$\begin{bmatrix} i_d(k+1) \\ i_q(k+1) \end{bmatrix} = A \begin{bmatrix} i_d(k) \\ i_q(k) \end{bmatrix} + B \begin{bmatrix} u_d(k) \\ u_q(k) \end{bmatrix} - \begin{bmatrix} 0 \\ \frac{\omega_1(k)\psi_{f1}+\omega_2(k)\psi_{f2}}{L_{q1}+L_{q2}} \end{bmatrix} T \tag{24}$$

where

$$A = \begin{bmatrix} 1 - T\frac{2R_s}{L_{d1}+L_{d2}} & T\frac{\omega_1(k)L_{q1}+\omega_2(k)L_{q2}}{L_{d1}+L_{d2}} \\ -T\frac{\omega_1(k)L_{d1}+\omega_2(k)L_{d2}}{L_{q1}+L_{q2}} & 1 - T\frac{2R_s}{L_{q1}+L_{q2}} \end{bmatrix}, \; B = \begin{bmatrix} \frac{T}{L_{d1}+L_{d2}} & 0 \\ 0 & \frac{T}{L_{q1}+L_{q2}} \end{bmatrix},$$

T is the control cycle, and $i_d(k+1)$ and $i_q(k+1)$ represent the predicted values of the *d*-axis and *q*-axis components of stator currents at time $k+1$.

The discrete output equation of the system is as follows:

$$y(k) = \begin{bmatrix} y_d(k) \\ y_q(k) \end{bmatrix} = \begin{bmatrix} 1 & 0 \\ 0 & 1 \end{bmatrix} \begin{bmatrix} i_d(k) \\ i_q(k) \end{bmatrix} \tag{25}$$

where $y_d(k)$ and $y_q(k)$ are the *d*-axis and *q*-axis output values of the system at time *k*, respectively.

Due to the significantly smaller electrical time constant compared to the mechanical time constant of the CRPMSM control system, it can be assumed that CRPMSM speed remains constant over multiple control cycles (i.e., $\omega_1(k) = \omega_1(k+1)$ and $\omega_2(k) = \omega_2(k+1)$). Using Equations (24) and (25), the CRPMSM incremental predictive model can be represented as shown in Equations (26) and (27).

$$\begin{bmatrix} \Delta i_d(k+1) \\ \Delta i_q(k+1) \end{bmatrix} = A \begin{bmatrix} \Delta i_d(k) \\ \Delta i_q(k) \end{bmatrix} + B \begin{bmatrix} \Delta u_d(k) \\ \Delta u_q(k) \end{bmatrix} \tag{26}$$

$$\begin{bmatrix} y_d(k) \\ y_q(k) \end{bmatrix} = \begin{bmatrix} 1 & 0 \\ 0 & 1 \end{bmatrix} \begin{bmatrix} \Delta i_d(k) \\ \Delta i_q(k) \end{bmatrix} + \begin{bmatrix} y_d(k-1) \\ y_q(k-1) \end{bmatrix} \tag{27}$$

where

$$\begin{cases} \Delta i_d(k) = i_d(k) - i_d(k-1) \\ \Delta i_q(k) = i_q(k) - i_q(k-1) \end{cases}, \begin{cases} \Delta u_d(k) = u_d(k) - u_d(k-1) \\ \Delta u_q(k) = u_q(k) - u_q(k-1) \end{cases}$$

Considering the computational load and response time of the CRPMSM control system, it is essential to determine the applicable sampling period while meeting control requirements. Therefore, selecting the appropriate prediction horizon p and control horizon m is crucial. The control process of CRPMSM involves four stages: the inverter generates voltage vectors, the voltage vectors are applied to the control system to obtain control variables, the control variables along with the currents are inputted into the prediction model to produce predicted currents, and the predicted currents are applied to CRPMSM to follow the set speed. The optimal voltage vector obtained in the k-th control cycle acts on the system, and the speed information of the CRPMSM corresponding to this voltage vector can only be obtained in the $k + 4$th control cycle. Therefore, the minimum prediction horizon in this study is set to 4, with a prediction horizon p and a control horizon m both equal to 4 for the controller.

Based on Equations (26) and (27), the predicted outputs for the next four control cycles can be calculated as follows:

$$\begin{bmatrix} y(k+1|k) \\ y(k+2|k) \\ y(k+3|k) \\ y(k+4|k) \end{bmatrix} = My(k) + S_I \begin{bmatrix} \Delta i_d(k) \\ \Delta i_q(k) \end{bmatrix} + S_u \begin{bmatrix} \Delta u(k) \\ \Delta u(k+1) \\ \Delta u(k+2) \\ \Delta u(k+3) \end{bmatrix} \tag{28}$$

where

$$S_I = \begin{bmatrix} CA \\ \sum_{i=1}^{2} CA^i \\ \sum_{i=1}^{3} CA^i \\ \sum_{i=1}^{4} CA^i \end{bmatrix}, S_u = \begin{bmatrix} CB_u & 0 & 0 & 0 \\ \sum_{i=1}^{2} CA^{i-1}B_u & CB_u & 0 & 0 \\ \sum_{i=1}^{2} CA^{i-1}B_u & \sum_{i=1}^{2} CA^{i-1}B_u & CB_u & 0 \\ \sum_{i=1}^{2} CA^{i-1}B_u & \sum_{i=1}^{2} CA^{i-1}B_u & \sum_{i=1}^{2} CA^{i-1}B_u & CB_u \end{bmatrix}, M = \begin{bmatrix} M_{2\times2} \\ M_{2\times2} \\ M_{2\times2} \\ M_{2\times2} \end{bmatrix},$$

$k + i \,|\, k$ represents the prediction from time k to $k + i$, with i taking values 1, 2, 3, and 4; and M is the ratio of the output values at time k to time $k-1$.

The cost function constructed in this study is expressed as Equation (29). The first term of the cost function aims to stabilize the stator currents to their expected values, while the second term limits control increments to prevent excessive voltage fluctuations.

$$J = \sum_{i=1}^{p} \sum_{j=1}^{n_y} \left\{ \Gamma_{y_j,i} \left[y_j(k+i|k) - r_j(k+i) \right] \right\}^2 + \sum_{i=1}^{m} \sum_{j=1}^{n_u} \left\{ \Gamma_{u_j,i} \Delta u_j(k+i-1) \right\}^2 \tag{29}$$

where n_y and n_u denote the maximum prediction lengths for model predictive output and control input, respectively; $r_j(k + i)$ represents the expected output value of the dq-axis current; $\Delta u_j(k + i-1)$ represents the control increment at time $k + i-1$; and $\Gamma y_j,i$ and $\Gamma u_j,i$ are the weighted coefficients for the j-th prediction control output error and the j-th component of the control increment, respectively.

According to Equation (30), the optimal solutions $\Delta u_d{}^*(k)$ and $\Delta u_q{}^*(k)$ to minimize the cost function can be obtained. By initializing the state and control variables to 0 and iteratively calculating $u_d(k)$ and $u_q(k)$ as in Equation (31), they are applied to CRPMSM control.

$$\frac{\partial J}{\partial \Delta u(k)} = 0 \tag{30}$$

$$\begin{cases} u_d(k) = \Delta u_d(k) + u_d(k-1) \\ u_q(k) = \Delta u_q(k) + u_q(k-1) \end{cases} \tag{31}$$

4.2. Implementation of MPC for CRPMSM

The flowchart of the MPC strategy for CRPMSM is depicted in Figure 6. The established block diagram of the MPC system for CRPMSM is illustrated in Figure 7. The control system employs the i_d = 0 control method and retains the speed proportional-integral (PI) controller. The predictive model and cost function constitute the model prediction controller, which replaces the traditional PI current loop in the VC strategy. The variables with asterisk represent reference values.

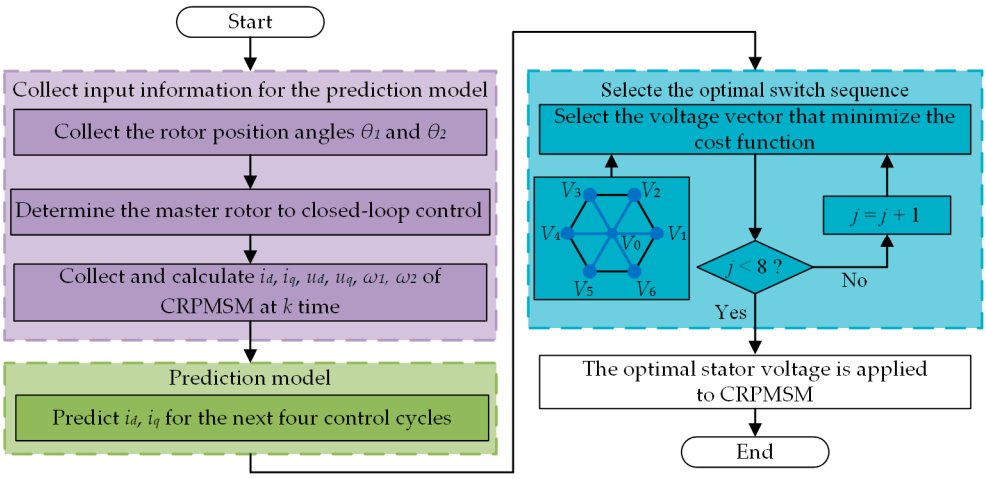


Figure 6. Flow chart of MPC strategy.

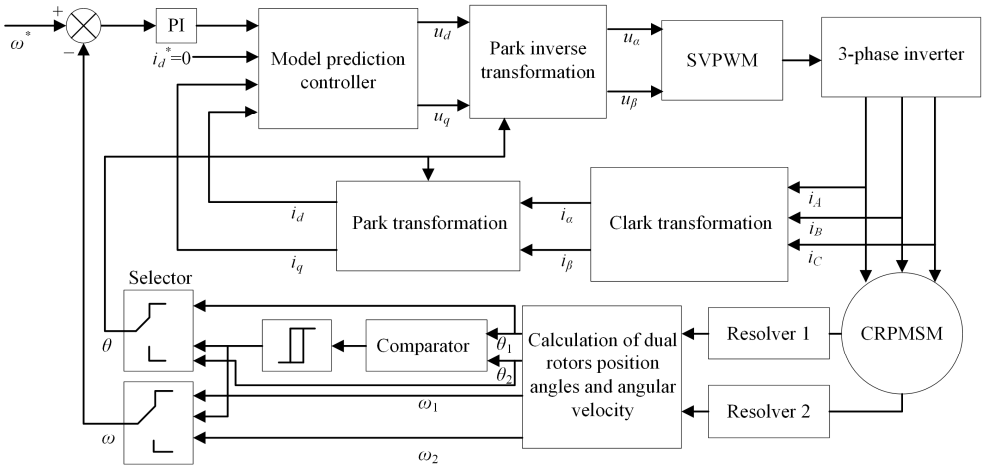


Figure 7. Block diagram of MPC system for CRPMSM.

The position angles of two rotors θ_1 and θ_2 are measured and then used to determine the master rotor to orient the rotor flux linkage, according to the master-slave control strategy in Section 3. Stator currents and voltages in the ABC coordinate system are measured with sensors and transformed into i_d, i_q, u_d and u_q in the d, q-axis coordinates. The predicted i_d and i_q for the next control cycles can be obtained by the established predict model, as expressed in Equation (24). Current increments of i_d and i_q are substituted into Equation (29) to evaluate the cost functions of seven different voltage vectors. The voltage vectors that minimize the cost function are selected. Finally, the inverter switching sequence associated with the optimal voltage vector is used to generate the required stator three-phase voltage and is applied to realize the control of CRPMSM.

5. Simulation Models for CRPMSM Control System

5.1. Simulation Model of CRPMSM

The simulation model for CRPMSM is illustrated in Figure 8. Input terminals 1 and 2 represent the load torques for rotor 1 and rotor 2 of CRPMSM. Input terminals 3, 4, and 5 correspond to the stator's three-phase voltages. Output terminal 1 represents the stator's three-phase currents, while output terminals 2 and 3 represent the speeds of rotor 1 and rotor 2. Output terminals 4 and 5 correspond to the electromagnetic torques of rotor 1 and rotor 2.

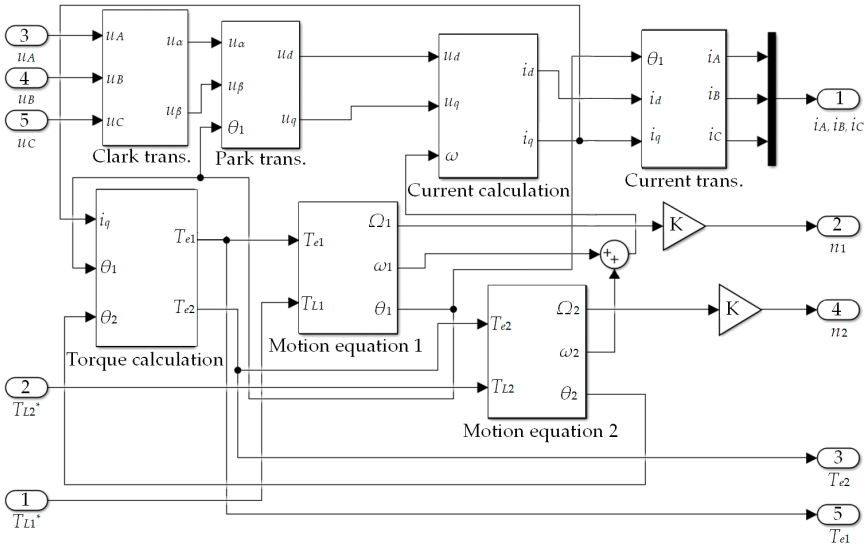


Figure 8. Simulation model of CRPMSM.

Using Clark and Park transformations, d-axis and q-axis voltage components can be obtained from the stator three-phase voltage applied to the CRPMSM. The angular velocities of two rotors, ω_{e1} and ω_{e2}, can be measured by resolvers. Combining with d, q-axis inductance, stator resistance, and PM flux linkage, and hence d-axis and q-axis currents can be obtained through the current calculation module, according to Equation (22). The stator three-phase currents are obtained from i_d, i_q, and the rotor position angles θ using a 2r/3s current transformation module. The electromagnetic torque of two rotors is calculated by i_q, θ_1 and θ_2 through the torque calculation module. Combining with the load torque used as the input of the motion equation module, the mechanical angular velocity ω_{m1} and ω_{m2} of two rotors are obtained, respectively, and converted into rotor speeds n_1 and n_2.

CRPMSMs require the real-time measurement of rotor position during operation, and the accuracy of measured rotor position has a significant effect on the performance of the motor system. The resolvers are used to measure the rotor positions in this study, which have the advantages of favorable environmental adaptability, fast response, and high reliability. The electromagnetic design, manufacturing process, and mechanical installation should be carefully considered in the design and employment of resolvers, which will cause errors in the measured rotor position.

5.2. Simulation Model of MPC Module

The simulation model of the MPC module is illustrated in Figure 9. It establishes the relationship between speed and q-axis current through the speed outer loop to obtain the q-axis current reference value i_q^*. The $i_d = 0$ control strategy is employed, and therefore the d-axis current reference value i_d^* is set as 0. The MPC module is implemented through programming. Firstly, seven inverter voltage vectors and the corresponding switching sequences are defined. Secondly, the inverter voltage vectors are converted into dq-axis voltage components. And then dq-axis currents and electrical angular velocity ω are

collected from the master-slave control module. The *dq*-axis currents for the next four control cycles are calculated using the predictive model. Finally, seven cost functions are computed, and the inverter switching sequence (S_a, S_b, S_c) that minimizes the cost function is selected. The switching sequence outputted by the MPC module undergoes space vector pulse width modulation (SVPWM) to generate the required stator's three-phase voltages, which serve as inputs to the CRPMSM module.

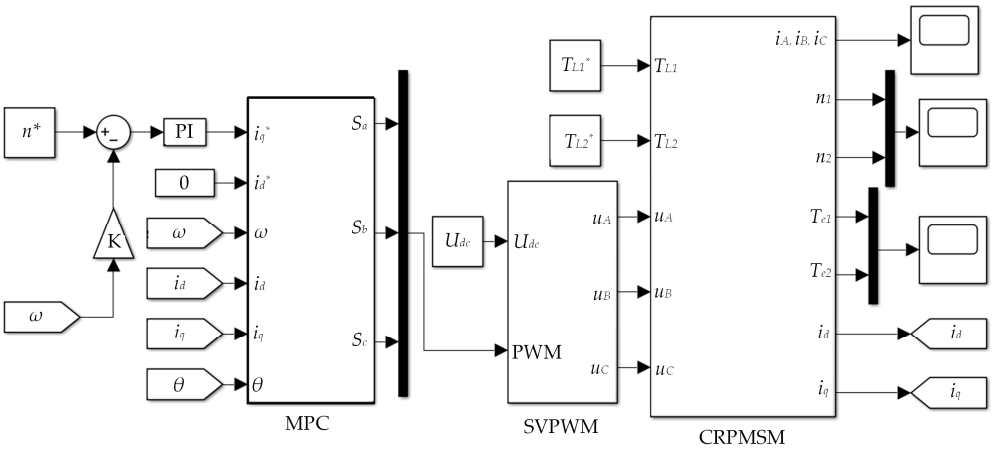


Figure 9. Simulation model of MPC module.

5.3. Simulation Model of Master-Slave Control Module

The electrical angular velocity ω and position angle θ are acquired from the master-slave control module, which is integrated within the CRPMSM module, and then ω and θ are transferred to the MPC module. The master-slave control module is shown in Figure 10.

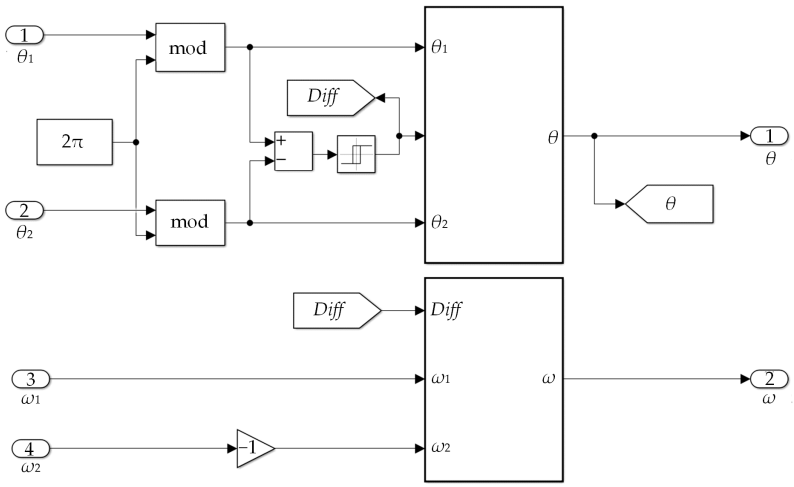


Figure 10. Master-slave control module.

The position angle of the dual rotor is subtracted by 2π modulus, and then used to generate the *Diff* signal through the hysteresis comparator. If *Diff* equals the upper output limit of the hysteresis comparator, it indicates that $\theta_1 > \theta_2$, and therefore Rotor 2 is selected as the master rotor, i.e., $\theta = \theta_2$ and $\omega = \omega_2$. Conversely, if $\theta_1 < \theta_2$, then the Rotor 1 is selected as the master rotor, and it can be obtained that $\theta = \theta_1$ and $\omega = \omega_1$.

6. Simulation Results and Analysis

The simulations and analyses are carried out to validate the effectiveness of the proposed MPC strategy for CRPMSM in scenarios involving balanced load variation, balanced speed variation, and unbalanced load variation, comparing it with the VC strategy. MATLAB/Simulink 2023 version is adopted to establish the model and realize the simulation of

the control strategy. The control effects are assessed on CRPMSM's speed, electromagnetic torque, and stator current under both MPC and VC strategies. The basic specifications of CRPMSM are presented in Table 1. A three-phase inverter with a bus voltage of 300 V and a switching frequency of 10 kHz is used as the power supply to simulate the CRPMSM control system.

Table 1. Specifications of CRPMSM.

Item	Value
Rated power	2 kW
Bus voltage	300 VDC
Rated current	14.14 A
Rated frequency	33.33 Hz
Rated speed	500 r/min
Rated torque	20 N·m
Number of pole pairs	4
Outer diameter	180 mm
Inner diameter	114 mm
Stator resistance	1.68 Ω
d, q-axis inductance	6.7 mH
Flux Linkage	0.1836 Wb
Moments of inertia	0.062 kg·m^2

The simulation model for CRPMSM with the VC strategy used for comparative analysis is depicted in Figure 11. In the VC simulation model for CRPMSM, the q-axis voltage reference value u_q^* is output based on the set speed through the speed and current control loops. Similarly, adopting the $i_d = 0$ control strategy, the d-axis voltage reference value u_d^* is output based on the expected d-axis current through the current control loops. The dq-axis voltage reference values and the rotor position angle θ are input into the voltage transformation module and SVPWM module to generate the stator's three-phase voltage. In contrast to the MPC simulation model, the VC simulation model for CRPMSM includes not only a speed closed-loop but also two current closed-loops.

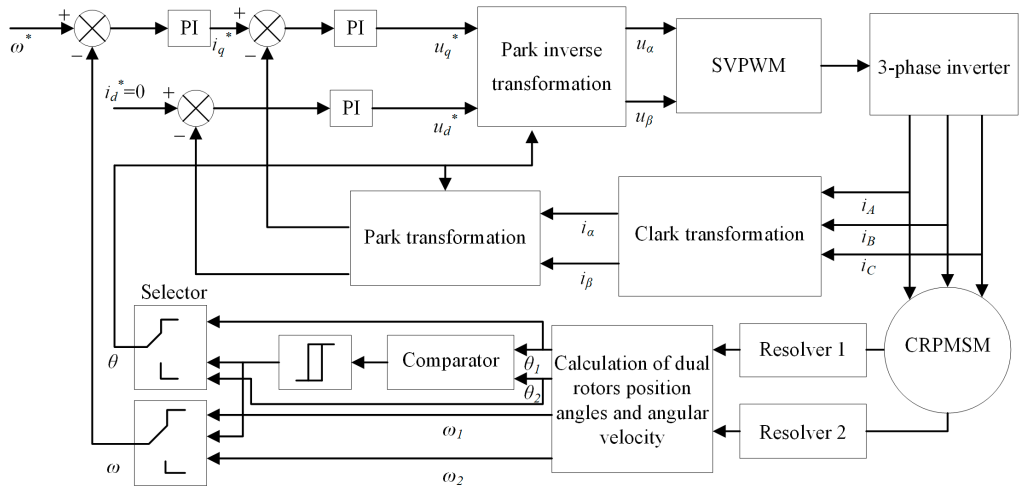


Figure 11. VC simulation model for CRPMSM.

6.1. Constant Speed with Balanced Load Variation

Both rotors of CRPMSM start with a balanced load torque of 10 N·m and the set speed is 300 r/min. At 0.2 s, the load torque for both rotors decreases to 5 N·m, and at 0.25 s, it returns to 10 N·m. The total simulation duration is 0.5 s. The speed response, electromagnetic torque response, and stator current are simulated for the CRPMSM using

the MPC strategy and the VC strategy, respectively, under the condition of balanced load variation. The simulation results are shown in Figures 12–14.

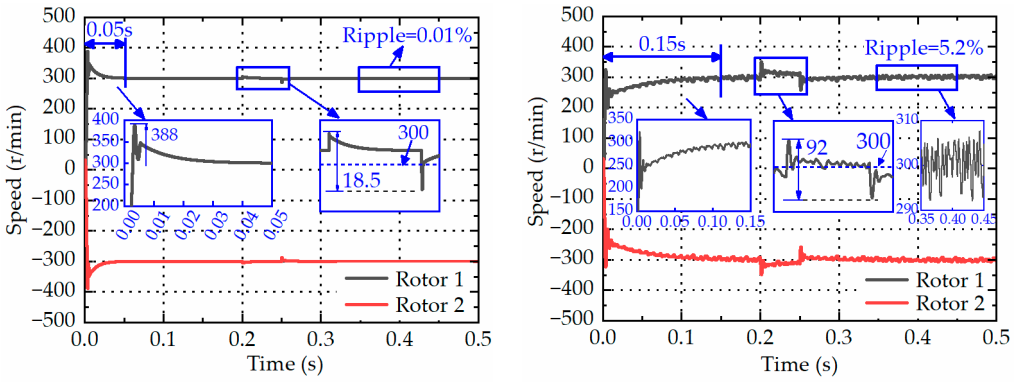


Figure 12. Speed response in the case of constant speed with balanced load variation. (**a**) MPC. (**b**) VC.

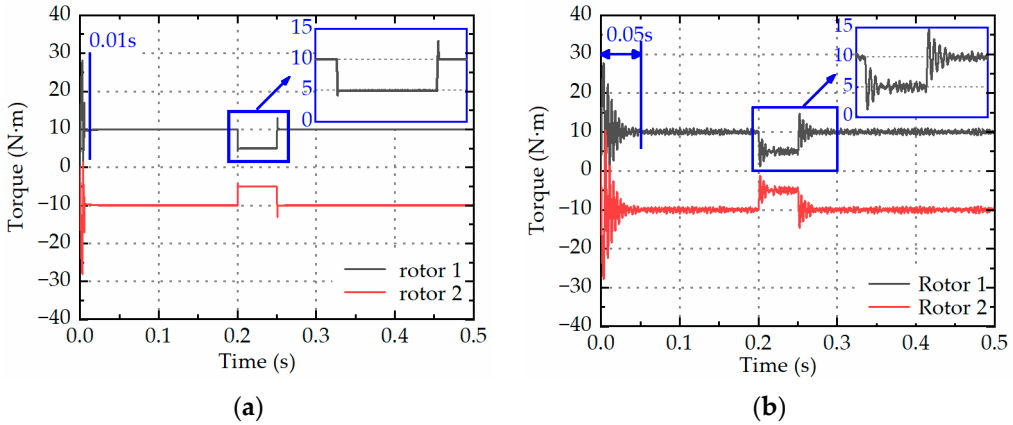


Figure 13. Electromagnetic torque response in the case of constant speed with balanced load variation. (**a**) MPC. (**b**) VC.

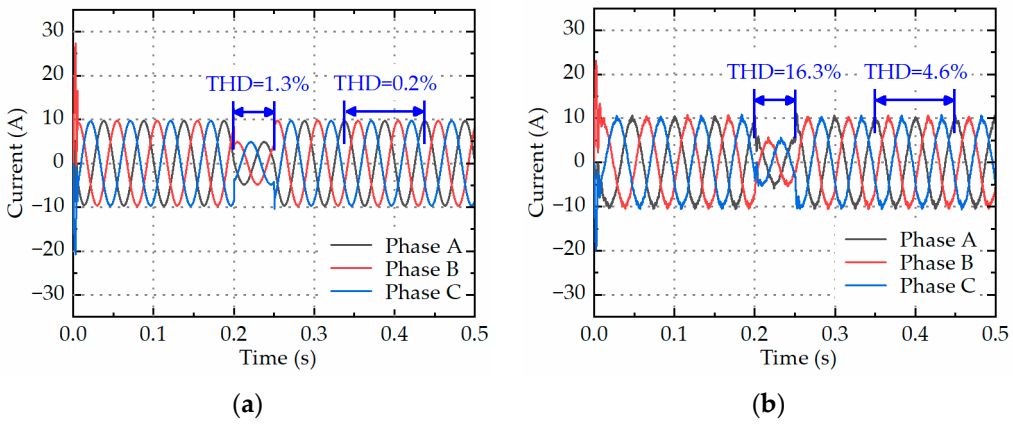


Figure 14. Current waveforms in the case of constant speed with balanced load variation. (**a**) MPC. (**b**) VC.

In Figure 12, it can be observed that CRPMSM, when controlled by MPC and VC, takes 0.05 s and 0.15 s, respectively, to transition from startup to stable operation. When the load balance changes, the speed ripples of CRPMSM under MPC and VC are 6.16% and 30.67%,

respectively. The CRPMSM using the MPC strategy exhibits more stable speed during the re-synchronization transition of both rotors compared to the VC strategy. Similarly, the speed ripple of CRPMSM using MPC and VC after re-synchronization is 0.01% and 5.2%, respectively, implying the superiority of the MPC strategy in speed control.

Figure 13 shows that the time required for the electromagnetic torque of CRPMSM to reach the stable value of 10 N·m is 0.01 s for the MPC strategy and 0.05 s for the VC strategy. The MPC strategy results in a faster dynamic response, as indicated by the faster stabilization of electromagnetic torque both in the startup period and the re-synchronization transition.

Figure 14 shows the stator current waveforms of the CRPMSM in the case of constant speed with balanced load variation, and Figure 15 shows the corresponding current spectra analysis for the re-synchronization transition and after re-synchronization. It can be found that during the re-synchronization transition, the stator currents decrease as the load torque undergoes a reduction. Compared to the VC strategy, the harmonic contents of stator current under the MPC strategy are much lower both during the period of re-synchronization and after the re-synchronization. In the re-synchronization transition, the harmonic content is higher than that after the synchronization for both the MPC strategy and the VC strategy. The harmonic distortion of stator current is 1.3% under the MPC strategy and 16.3% under the VC strategy in the re-synchronization transition, while it is 0.2% and 4.6% for the MPC strategy and VC strategy after re-synchronization, respectively. The MPC strategy exhibits significantly reduced harmonic content in stator currents.

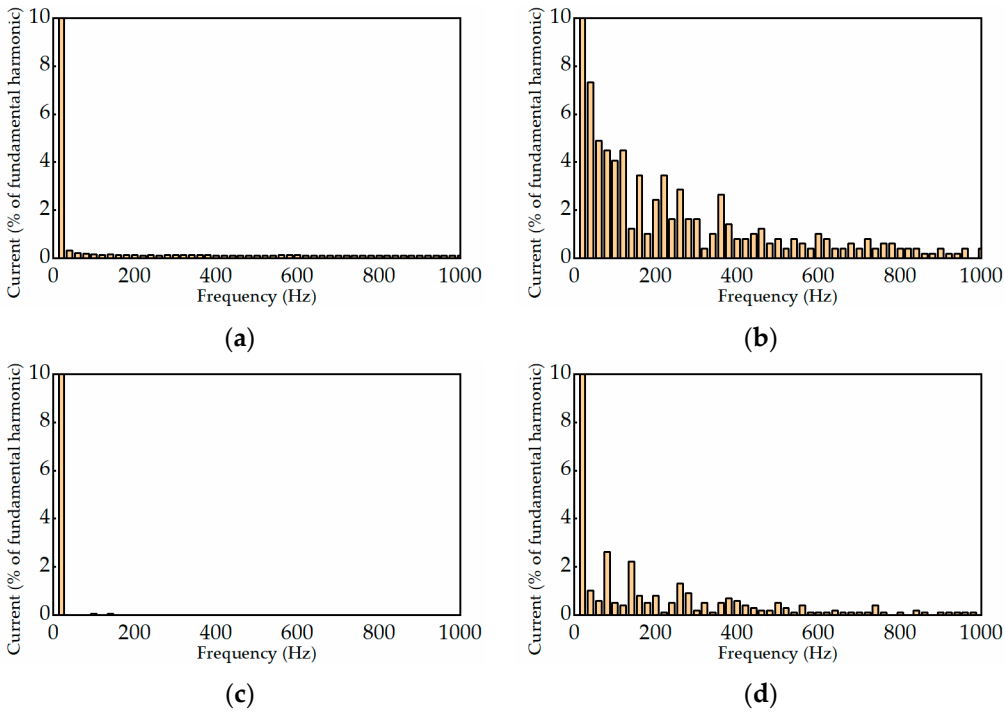
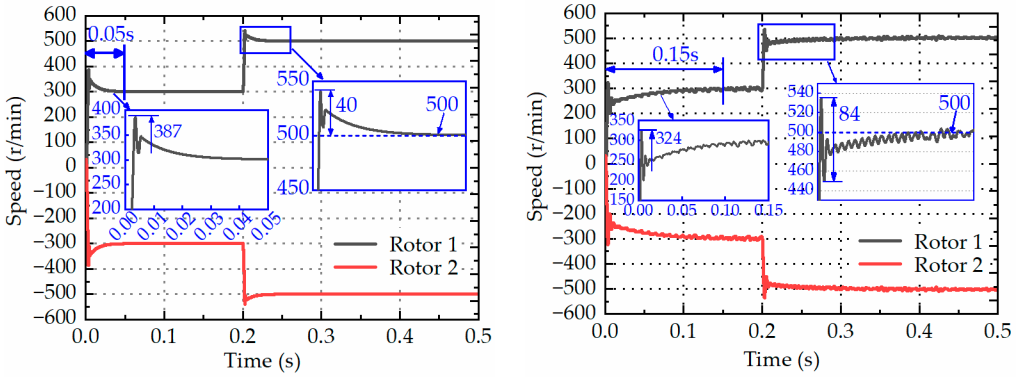


Figure 15. Current spectra in the case of constant speed with balanced load variation. (**a**) In re-synchronization transition for MPC. (**b**) In re-synchronization transition for VC. (**c**) After re-synchronization for MPC. (**d**) After re-synchronization for VC.

6.2. Balanced Speed Variation with Load Unchanged

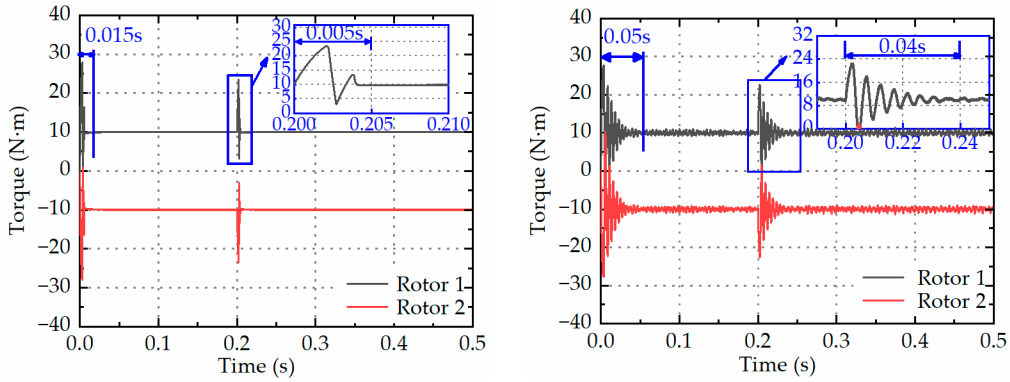
Both rotors of CRPMSM start with a balanced load torque of 10 N·m, and at 0.2 s, the speed of CRPMSM increases from 300 r/min to 500 r/min. The speed, electromagnetic torque, and stator current of CRPMSM controlled by MPC strategy and VC strategy during speed changes are shown in Figures 16–18. Figure 16 indicates that CRPMSM takes 0.05 s and 0.15 s for MPC strategy and VC strategy, respectively, to elevate the motor speed from 0 r/min to the given speed. The MPC strategy achieves stable operation in less time and

with smoother speed control. During sudden changes in the set speed, MPC strategy results in speed fluctuations of 8.0%, while VC strategy exhibits fluctuations of 16.8%.



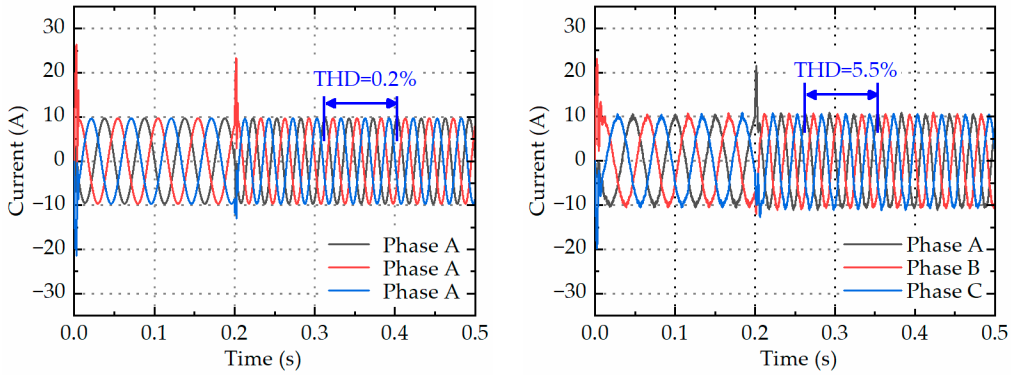
(**a**) (**b**)

Figure 16. Speed response in the case of balanced speed variation with load unchanged. (**a**) MPC. (**b**) VC.



(**a**) (**b**)

Figure 17. Electromagnetic torque response in the case of balanced speed variation with load unchanged. (**a**) MPC. (**b**) VC.



(**a**) (**b**)

Figure 18. Current waveforms in the case of balanced speed variation with load unchanged. (**a**) MPC. (**b**) VC.

Figure 17 demonstrates that after the set speed sudden changes, MPC strategy and VC strategy take 0.005 s and 0.04 s, respectively, to stabilize the electromagnetic torque of CRPMSM back to 10 N·m. The MPC strategy exhibits shorter recovery times for electromagnetic torque, indicating a faster dynamic response. Figure 18 illustrates that the stator

current of CRPMSM under the MPC strategy is smoother. FFT analysis shows that when CRPMSM's speed changes and stabilizes at 500 r/min, the harmonic distortion of the stator current is 0.2% under the MPC and 5.5% under the VC. This analysis reveals that CRPMSM under the MPC strategy has superior dynamic performance and less harmonic loss when the speed changes suddenly.

6.3. Unbalanced Load Variation

Both rotors of CRPMSM start with a balanced load torque of 10 N·m and the set speed is 300 r/min. At 0.2 s, the load torque of rotor 1 suddenly decreases to 6 N·m, which acts as the master rotor, and the load of rotor 2 decreases to 5 N·m, which acts as the slave rotor. At 0.25 s, both rotor loads simultaneously return to 10 N·m. MPC strategy and VC strategy are utilized to analyze the effects of unbalanced load variation on CRPMSM's speed, electromagnetic torque, and stator current, as shown in Figures 19–21.

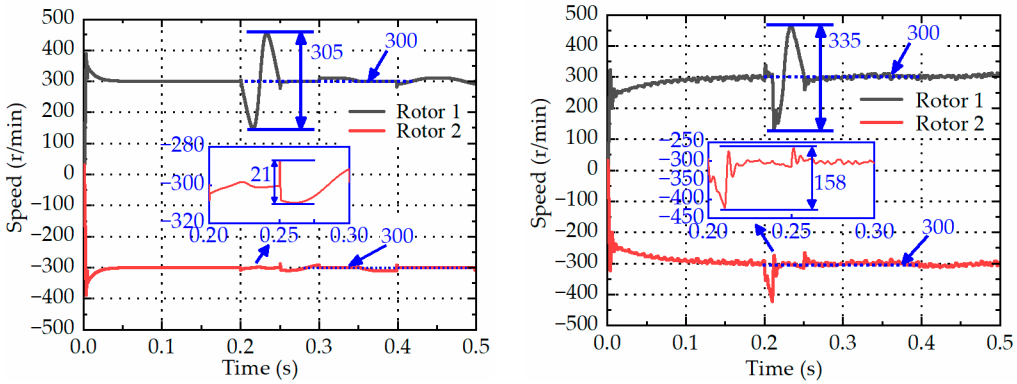


Figure 19. Speed response in the case of unbalanced load variation. (**a**) MPC. (**b**) VC.

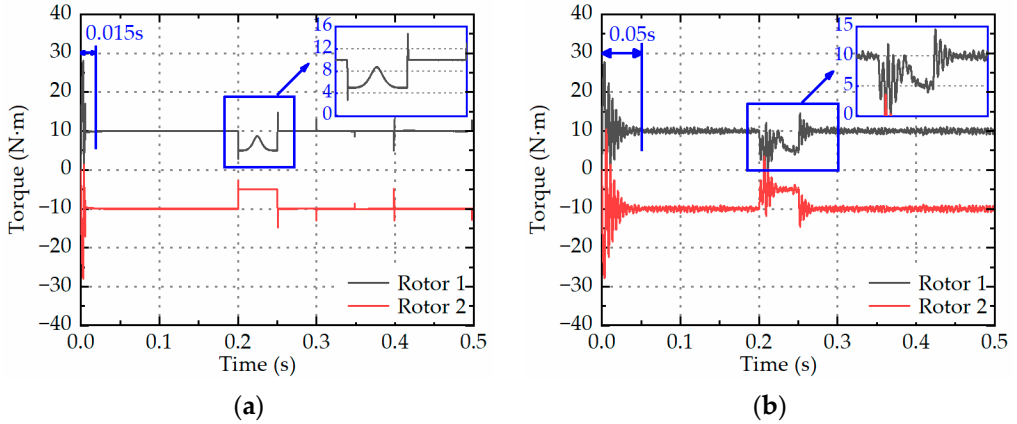


Figure 20. Electromagnetic torque response in the case of unbalanced load variation. (**a**) MPC. (**b**) VC.

In Figure 19, before the load imbalance changes, CRPMSM under the MPC strategy can reach and stabilize at the given speed more quickly. During load imbalance changes in CRPMSM under the MPC strategy, the speed ripple of the master rotor is 101.7% and that of the slave rotor is 7.0%. While for the CRPMSM under the VC strategy, the speed ripple of the master rotor is 111.7% and that of the slave rotor is 52.7%. The MPC strategy results in a much smaller speed ripple and a shorter time to reach stability.

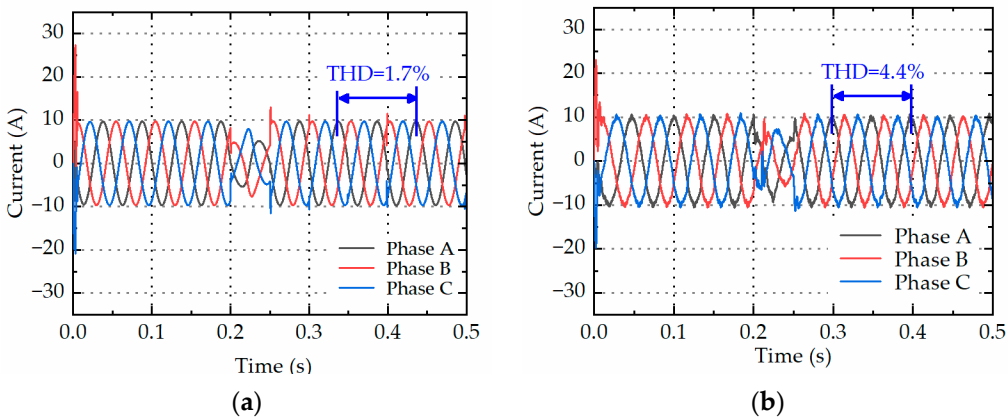


Figure 21. Current waveforms in the case of unbalanced load variation. (**a**) MPC. (**b**) VC.

Figure 20 shows that when load imbalance occurs, the electromagnetic torque fluctuations of CRPMSM under MPC strategy and VC strategy are 120% and 314%, respectively. The use of MPC significantly reduces electromagnetic torque fluctuations in the motor. Figure 21 reveals that the stator current of CRPMSM is smoother when controlled by the MPC strategy. FFT analysis shows that when CRPMSM reaches stable operation after load variation, the harmonic distortion of stator current under the MPC and VC is 1.7% and 4.4%, respectively. This analysis demonstrates that CRPMSM exhibits better dynamic performance under the MPC strategy when subjected to load imbalance changes, addressing the issues of significant speed ripples and long transition times observed under the VC strategy.

7. Conclusions

In this paper, the MPC strategy is employed to address the issue of speed fluctuations caused by load variation in CRPMSM. The speed response, electromagnetic torque, and stator current are simulated for the CRPMSM under the MPC strategy and compared to the VC strategy. Compared to the VC strategy, the speed ripple of CRPMSM using the MPC strategy in the condition of load balanced change can be decreased from 30.67% to 6.16%, while using the MPC strategy it can be decreased from 16.8% to 8.0% in the condition of speed-balanced change. When the CRPMSM involves unbalanced load variation, the master rotors in two control methods both have a relatively large speed ripple, while the slave rotor under the MPC strategy achieves a significant reduction in speed ripple, which decreases from 52.7% to 7%. The results show that CRPMSM controlled by MPC exhibits smaller speed ripples and faster re-synchronization when subjected to changes in load and speed. In all studied conditions, the stator current THDs of the CRPMSM using the MPC strategy are apparently lower than those under the VC strategy, which can help alleviate the harmonic loss of the motor.

Author Contributions: Conceptualization, S.Z.; methodology, S.Z. and Y.N.; validation, Y.N. and Y.Z.; formal analysis, Y.N. and Y.Z.; investigation, S.Z. and Y.N.; writing—original draft preparation, Y.N. and Y.Z.; writing—review and editing, S.Z. and M.T.V.; supervision, S.Z. and C.X.; funding acquisition, C.X. and M.T.V. All authors have read and agreed to the published version of the manuscript.

Funding: This research was funded by the National Key Research and Development Program of China, grant number 2023YFB4301500.

Institutional Review Board Statement: Not applicable.

Informed Consent Statement: Not applicable.

Data Availability Statement: Data are contained within the article.

Conflicts of Interest: The authors declare no conflicts of interest.

References

1. Jiang, H.; Ouyang, W.; Sheng, C.X.; Lan, J.F.; Bucknall, R. Numerical investigation on hydrodynamic performance of a novel shaftless rim-driven counter-rotating thruster considering gap fluid. *Appl. Ocean Res.* **2022**, *118*, 102967. [CrossRef]
2. Capone, A.; Felice, F.D.; Pereira, F.A. On the flow field induced by two counter-rotating propellers at varying load conditions. *Ocean Eng.* **2021**, *221*, 108322. [CrossRef]
3. Pereira, F.A.; Capone, A.; Felice, F.D. Flow field and vortex interactions in the near wake of two counter-rotating propellers. *Appl. Ocean Res.* **2021**, *117*, 102918. [CrossRef]
4. Ma, J.D.; Wu, B.; Zargari, N.R.; Rizzo, S.C. A space vector modulated csi-based ac drive for multimotor applications. *IEEE Trans. Power Electron.* **2001**, *16*, 535–544. [CrossRef]
5. Matsuse, K.; Kouno, Y.; Kawai, H.; Yokomizo, S. A speed-sensorless vector control method of parallel-connected dual induction motor fed by a single inverter. *IEEE Trans. Ind. Appl.* **2002**, *38*, 1566–1571. [CrossRef]
6. Bidart, D.; Pietrzak-David, M.; Maussion, P.; Fadel, M. Mono inverter dual parallel pmsm-structure and control strategy. In Proceedings of the 34th IEEE Industrial Electronics Conference, Orlando, FL, USA, 10–13 November 2008.
7. Xu, F.; Shi, L.M.; Li, Y.H. The weighted vector control of speed-irrelevant dual induction motors fed by the single inverter. *IEEE Trans. Power Electron.* **2013**, *28*, 5665–5672. [CrossRef]
8. Bouscayrol, A.; Pietrzak-David, M.; Delarue, P.; Pena-Eguiluz, R.; Vidal, P.E.; Kestelyn, X. Weighted control of traction drives with parallel-connected ac machines. *IEEE Trans. Ind. Electron.* **2006**, *53*, 1799–1806. [CrossRef]
9. Matsuse, K.; Kawai, H.; Kouno, Y.; Oikawa, J. Characteristics of speed sensorless vector controlled dual induction motor drive connected in parallel fed by a single inverter. *IEEE Trans. Ind. Appl.* **2004**, *40*, 153–161. [CrossRef]
10. Cheng, S.Y.; Luo, D.R.; Huang, S.D.; Chen, Z.; Huang, K.Y. Control strategy for permanent magnet synchronous motor with contra-rotating rotors under unbalanced loads condition. *IET Electr. Power Appl.* **2015**, *9*, 71–79. [CrossRef]
11. Rao, Z.M.; Huang, S.D.; Luo, D.R.; Jiang, Y.; Cheng, S.Y.; Huang, Z. Analysis and direct torque control of a disc permanent magnet synchronous motor for contra-rotating propellers. *Proc. CSEE* **2019**, *39*, 5225–5236. (In Chinese)
12. Zhong, Y.C.; Huang, S.D.; Luo, D.R.; He, R.Z. Speed synchronism of permanent magnet synchronous motor with dual contra-rotating rotors under load variation. *IET Power Electron.* **2017**, *10*, 1479–1486. [CrossRef]
13. Liu, X.D.; Yu, H.S.; Yu, J.P.; Zhao, L. Combined speed and current terminal sliding mode control with nonlinear disturbance observer for pmsm drive. *IEEE Access* **2018**, *6*, 29594–29601. [CrossRef]
14. Wang, A.M.; Jia, X.W.; Dong, S.H. A new exponential reaching law of sliding mode control to improve performance of permanent magnet synchronous motor. *IEEE Trans. Magn.* **2013**, *49*, 2409–2412. [CrossRef]
15. Hsien, T.L.; Sun, Y.Y.; Tsai, M.C. H∞ control for a sensorless permanent-magnet synchronous drive. *IEE Proc. Electr. Power Appl.* **1997**, *144*, 173–181. [CrossRef]
16. Feng, G.; Liu, Y.F.; Huang, L.P. A new robust algorithm to improve the dynamic performance on the speed control of induction motor drive. *IEEE Trans. Power Electron.* **2004**, *19*, 1614–1627. [CrossRef]
17. Chen, C.S. Tsk-type self-organizing recurrent-neural-fuzzy control of linear microstepping motor drives. *IEEE Trans. Power Electron.* **2010**, *25*, 2253–2265. [CrossRef]
18. Singh, M.; Chandra, A. Application of adaptive network-based fuzzy inference system for sensorless control of pmsg-based wind turbine with nonlinear-load-compensation capabilities. *IEEE Trans. Power Electron.* **2011**, *26*, 165–175. [CrossRef]
19. Luo, D.R.; He, R.Z.; Huang, S.D.; Su, X. Optimized vector control strategy for contra-rotating permanent magnet synchronous motor under serious unbalanced load adopting torque compensation. In Proceedings of the 22nd International Conference on Electrical Machines and Systems, Harbin, China, 11–14 August 2019; pp. 1–6.
20. Luo, D.R.; Su, X.; He, R.Z.; Huang, S.D. Dual-rotor direct torque control strategy of disk-type contra-rotating permanent magnet synchronous motor under heave unbalanced load torque. *Trans. China Electrotech. Soc.* **2019**, *34*, 4678–4686. (In Chinese)
21. Li, S.H.; Zhou, M.M.; Yu, X.H. Design and implementation of terminal sliding mode control method for pmsm speed regulation system. *IEEE Trans. Ind. Inform.* **2013**, *9*, 1879–1891. [CrossRef]
22. Zhang, X.G.; Sun, L.Z.; Zhao, K.; Sun, L. Nonlinear speed control for pmsm system using sliding-mode control and disturbance compensation techniques. *IEEE Trans. Power Electron.* **2013**, *28*, 1358–1365. [CrossRef]

Disclaimer/Publisher's Note: The statements, opinions and data contained in all publications are solely those of the individual author(s) and contributor(s) and not of MDPI and/or the editor(s). MDPI and/or the editor(s) disclaim responsibility for any injury to people or property resulting from any ideas, methods, instructions or products referred to in the content.